Combustion synthesized copper-ion substituted $FeAl_2O_4$ ($Cu_{0.1}Fe_{0.9}Al_2O_4$): A superior catalyst for methanol steam reforming compared to its impregnated analogue

Sayantani Maiti[a], Jordi Llorca[b], Montserrat Dominguez[b], Sara Colussi[c], Alessandro Trovarelli[c], Kaustubh R. Priolkar[d], Giuliana Aquilanti[e] and Arup Gayen[a,*]

[a]Department of Chemistry, Jadavpur University, Kolkata 700032, India

[b]Institut de Tècniques Energètiques and Centre for Research in Nanoengineering, Universitat Politècnica de Catalunya, 08028 Barcelona, Spain

[c]Dipartimento di Chimica, Fisica e Ambiente, Università di Udine, 33100 Udine, Italy

[d]Department of Physics, Goa University, Goa 403206, India

[e]Elettra-Sincrotrone Trieste S.C.p.A., s.s. 14, km 163.5 I-34149 Basovizza, Trieste, Italy

---

[*]Corresponding author; e-mail: agayenju@yahoo.com

Ph: +91-33-2457-2767; Fax: +91-33-2414-6223

Abstract

A series of copper ion substituted MAl_2O_4 (M= Mg, Mn, Fe and Zn) spinels is prepared by a single step solution combustion synthesis (SCS) and tested for methanol steam reforming (MSR). The copper ion substituted $Cu_{0.1}Fe_{0.9}Al_2O_4$ appears to be the most active, showing ~98% methanol conversion at 300 °C with ~5% CO selectivity at GHSV= 30000 h^{-1} and H_2O:CH_3OH= 1.1. The analogous impregnated catalyst, CuO (10 at.%)/$FeAl_2O_4$, is found to be much less active. These materials are characterized by XRD, H_2-TPR, BET, HRTEM, XPS and XANES analyses. Spinel phase formation is highly facilitated upon Cu-ion substitution, and Cu loading beyond 10 at.% leads to the formation of CuO as an additional phase. The ionic substitution of copper in $FeAl_2O_4$ leads to the highly crystalline SCS catalyst containing Cu^{2+} ion sites that are shown to be more active than the dispersed CuO nano-crystallites on the $FeAl_2O_4$ impregnated catalyst, despite its lower surface area. The as prepared SCS catalyst contains also a portion of copper as Cu^{1+} that increases when subjected to reforming atmosphere. The MSR activity of the SCS catalyst decreases with time-on-stream due to the sintering of catalyst crystallites as established from XPS and HRTEM analyses.

Keywords: Copper; $FeAl_2O_4$; Ionic substitution; Methanol steam reforming; Solution combustion; Impregnation

1. Introduction

The depletion of fossil fuel resources with the increasing demand of clean energy sources has driven the research attention for the search of suitable alternatives. A great opportunity to reduce the emission of toxic compounds such as nitrogen oxides, carbon oxides, various hydrocarbons etc. is given by the application of fuel cells which are energetically efficient and have minimum environmental impact. More specifically, for power generation as well as transport applications, polymer electrolyte membrane fuel cells (PEMFC) are suitable devices [1]. The production of clean hydrogen (<10 ppm CO) is the main requirement for PEMFC application, together with the overcoming of the issues related to hydrogen storage and distribution [2, 3]. The metallic hydrides can be a possible source of hydrogen during transportation, but a practical storage possibility is far from reality [4]. Reforming reactions have been shown to be effective for on-board hydrogen generation and thus can solve the transportation problems [5-9]. In comparison to the other sources, hydrogen production from alcohols has become a matter of great interest, methanol being the most favorable source due to its various advantages [3, 4, 10]. Although in most of the cases methanol is produced from natural gas, it can also be derived from renewable sources thus lowering the amount of carbon dioxide in the environment [11].

Besides methanol steam reforming (MSR; Eq. (1)), hydrogen is produced via two side reactions; thermal decomposition of methanol (MD; Eq. (2)) and water gas shift reaction (WGS; Eq. (3)) [12, 13]:

$$CH_3OH + H_2O \rightarrow 3H_2 + CO_2 \qquad \Delta H^0 = 49.7 \text{ kJ mol}^{-1} \qquad (1)$$

$$CH_3OH \rightarrow CO + 2H_2 \qquad \Delta H^0 = 90.2 \text{ kJ mol}^{-1} \qquad (2)$$

$$CO + H_2O \rightarrow CO_2 + H_2$$

$$\Delta H^0 = -41.2 \text{ kJ mol}^{-1} \quad (3)$$

The spinel type oxide materials are a hot topic of research owing to their very interesting properties that include high mechanical resistance, high thermal stability, low temperature sinterability, low surface acidity and high ability of cation diffusion [14]. These materials exhibit high performance in various reactions like water gas shift [15]; CO oxidation [16]; dehydrogenation of ethylbenzene [17]; steam reforming of dimethyl ether [18-20]; ethanol [21-23] and methanol [19, 24-35].

Now, the spinels having composition AB_2O_4 consist of a divalent metal ion (A^{2+}) usually occupying a tetrahedral site and a trivalent metal ion (B^{3+}) normally occupying the octahedral sites of a cubic oxide lattice. Hence it would be interesting to see if the Cu^{2+} ion can be stabilized within the oxide lattice structure and how that affects the MSR activity of the resulting copper-spinel oxide. The trivalent metal ions can also effectively prevent copper sintering which is mainly due to the agglomeration of Cu-particles [36]. A drawback of the spinel based catalysts is the low surface area caused primarily by the high calcination temperatures required for the spinel phase formation that restricts the availability of the active sites [18-20, 34]. The surface area and other properties can be improved by using different and/or a combination of different synthetic routes.

$CuAl_2O_4$ prepared by the coprecipitation method performs well towards MSR due to the formation of highly dispersed copper [24]. The Cu-Mn spinel oxide synthesized via the urea-nitrate combustion method has shown very good MSR activity due to the presence of variable oxidation states of both copper and manganese [25, 26]. The reduced Cu-Mn spinel oxide is much more reactive than the reduced Cu-Mn non-spinel mixed oxide due to the higher Cu-metal dispersion with smaller particle size of copper on spinel [27]. High methanol conversion

recorded over $CuFe_2O_4$ and $CuMn_2O_4$ spinels prepared by citric acid complex method as compared to the commercial catalyst $Cu/ZnO/Al_2O_3$ has been attributed to the enhancement of the stability of Cu^{1+} by the presence of neighboring MnO and Fe_3O_4 [19]. The spinel structure of $CuFe_2O_4$ is a key factor for the high MSR activity of $CuFe_2O_4/SiO_2$ synthesized by incipient wetness impregnation (IWI) method in reference to Cu/SiO_2 and Fe/SiO_2. The presence of iron inhibits Cu-sintering even after extensive H_2 reduction and the spinel has the ability to regenerate completely through air calcination due to the favorable phase transition from $CuFe_2O_4$ to Cu and Fe_3O_4, and again to $CuFe_2O_4$ [28]. Also the increased dispersion of copper through the reduction of rod like $CuFe_2O_4$ shows a high catalytic activity for MSR [29]. The spinel structure of $ZnAl_2O_4$ has controlling effect on the activity of $Cu/ZnAl_2O_4$ synthesized by the impregnation method due to the highly stabilized Cu^{1+} species on the surface of the support [30]. Also the incorporation of Cu^{2+} in to $ZnAl_2O_4$ is shown to be very effective for MSR [35]. Interestingly, the simultaneous presence of the $CuAl_2O_4$ spinel phase with a small portion of CuO made via a solid-phase method has been shown to possess an excellent catalytic performance in MSR [31]. A very high surface area $CuMn_2O_4$ spinel prepared by a silica aquagel confined precipitation method has also been shown to be a highly active MSR catalyst [32], as well as the synthesis of low surface area CuX_2O_4 (X= Mn, Fe, Al and La) spinels via a solid state route [33].

Most of the reported spinel systems suffer from phase decomposition after the reductive pretreatment or after the MSR treatment, thus the development of spinel oxides with a stable structure would be a very important result in the field of reforming reactions. In a recent paper, we have shown that $Cu_{0.03}Fe_{0.97}Al_2O_4$, is a highly efficient catalyst for the liquid phase oxidation of cyclohexane [37]. In this work we report for the first time the MSR behavior of copper ion substituted $FeAl_2O_4$ spinel oxides, $Cu_xFe_{1-x}Al_2O_4$ (x= 0.05, 0.07, 0.10 and 0.15) prepared by a

single step solution combustion synthesis (SCS). Our results show that $Cu_{0.1}Fe_{0.9}Al_2O_4$ is a promising catalyst for MSR showing better activity than (i) the combustion synthesized Cu (10 at.%) loaded $MgAl_2O_4$, $MnAl_2O_4$ and $ZnAl_2O_4$ spinels, (ii) the corresponding impregnated catalyst and (iii) some of the reported spinel catalysts in the literature.

2. Experimental

2.1. Preparation of materials

Pure $FeAl_2O_4$ and copper ion substituted $FeAl_2O_4$ spinels, $Cu_xFe_{1-x}Al_2O_4$ (x= 0.05, 0.07, 0.10 and 0.15; named as CuFeAlx (x= 5, 7, 10 and 15)) were prepared by the single step solution combustion of an aqueous stoichiometric redox mixture of the respective metal nitrate salts with the organic fuel oxalyldihydrazide ($C_2H_6N_4O_2$, ODH) in a muffle furnace as reported earlier [37]. The preparation of $Cu_{0.1}Fe_{0.9}Al_2O_4$ involves the combustion of the metal nitrates $Al(NO_3)_3.9H_2O$, $Fe(NO_3)_3.9H_2O$, $Cu(NO_3)_2.3H_2O$ with ODH, taken in a molar ratio 2: 0.9: 0.1: 4.45, at the ignition temperature of the redox mixture (~350 °C). In a typical synthesis, 5 g of $Al(NO_3)_3.9H_2O$ (Merck India, 99.9%), 2.4232 g of $Fe(NO_3)_3.9H_2O$ (Merck India, 99.9%), 0.161 g of $Cu(NO_3)_2.3H_2O$ (Merck India, 99.9%) and 3.506 g of ODH are dissolved in ~30 mL of double distilled water and then transferred to a preheated muffle furnace for the completion of combustion. The solution boils with frothing and foaming then it burns with a few sparks yielding a solid product within few minutes.

In order to assess the MSR activity behavior of copper loaded on the other spinel oxides, 10 at.% copper loaded on $MgAl_2O_4$, $MnAl_2O_4$ and $ZnAl_2O_4$ spinels has been prepared in a similar manner. The resulting materials have been named as CuMAl10 (M= Mg, Mn and Zn).

For the preparation of the impregnated catalyst, CuO (10 at.%)/$FeAl_2O_4$, the required amount of copper was deposited by incipient wetness impregnation of copper nitrate solution over combustion synthesized $FeAl_2O_4$ previously calcined at 400 °C for 3 h. The sample was then dried overnight at 100 °C and calcined at 400 °C for 3 h in air to obtain the impregnated catalyst (named as CuFeAl10IWI).

2.2. Characterization of materials

The powder X-ray diffraction (PXRD) data were collected on a Bruker D8 Advance X-ray diffractometer using Cu Kα radiation (λ= 1.5418 Å) generated at 40 kV and 40 mA. The PXRD patterns were recorded in the 2θ range of 10–100° using Lynxeye detector with a step size of 0.02° and scan time of 1 s per step. Average crystallite sizes were calculated from the line broadening of the PXRD peaks using Scherrer's equation.

BET surface areas were measured in a TriStar3000 porosimeter (Micromeritics). Before each measurement, the samples were degassed at 150 °C in vacuum for 90 min.

Temperature Programmed Reduction (H_2-TPR) experiments were carried out in a Micromeritics Autochem apparatus under a mixture of 5% H_2 in N_2 heating 40 mg of sample up to 1000 °C at a heating rate of 10 °C min^{-1}. Prior to the TPR measurements, the samples were pretreated for 1 h at 350 °C in air in order to clean the catalyst surface. Additional TPR experiments were conducted with the aim of getting some insights into the catalyst structure of selected samples during reduction. For this purpose the TPR experiments were stopped at selected temperatures (T= 350, 700 or 1000 °C), the gas was switched to pure nitrogen and the

reactor was quickly cooled to room temperature. The samples so obtained were then collected for X-ray analysis and are denoted as red@T, where T is the temperature reached during reduction.

The microstructural characterization by High Resolution Transmission Electron Microscopy (HRTEM) was performed at an accelerating voltage of 200 kV in a JEOL 2010F instrument equipped with a field emission source. The point-to-point resolution was 0.19 nm, and the resolution between lines was 0.14 nm. The magnification was calibrated against a Si standard. No induced damage of the samples was observed under prolonged electron beam exposure. The samples were dispersed in alcohol in an ultrasonic bath, and a drop of the supernatant suspension was poured onto a holey carbon-coated grid. The images were not filtered or treated by means of digital processing and they correspond to the raw data.

The surface characterization was done with X-ray photoelectron spectroscopy (XPS) on a SPECS system equipped with an Al anode XR50 source operating at 150 mW and a Phoibos 150 MCD-9 detector. The pressure in the analysis chamber was always below 10^{-7} Pa. The area analyzed was about 2 mm × 2 mm. The pass energy of the hemispherical analyzer was set at 25 eV and the energy step was set at 0.1 eV. The charge stabilization was achieved by using a SPECS Flood Gun FG 15/40. The sample powders were pressed to self-consistent disks for XPS analysis. The following sequence of spectra was recorded: survey spectrum, C 1s, Cu 2p, Fe 2p, Al 2p, Cu LMM Auger and C 1s again to check for charge stability as a function of time and the absence of degradation of the sample during the analyses. Data processing was performed with the CasaXPS program (Casa Software Ltd., UK). Binding energy (BE) values were centered using the C 1s peak at 284.8 eV. The atomic fractions (%) were calculated using peak areas normalized on the basis of acquisition parameters after background subtraction, experimental sensitivity factors and transmission factors provided by the manufacturer.

In situ MSR experiments were performed in a reaction chamber connected to the XPS analysis chamber that allowed treatments up to 600 °C and atmospheric pressure and sample transfer without exposure to air. The temperature of the sample was measured with a thermocouple in contact with the sample holder, which was heated with an IR lamp. Calcination treatments have been performed under synthetic air. The occurrence of the reaction/treatment during the *in situ* experiments (0-100 amu) was followed by an AMETEK mass spectrometer. Gases were introduced by means of mass flow controllers and water and methanol were introduced by bubbling the appropriate amount of carrier gas (Ar) to attain steam/methanol ratio (S/M)= 1.1 (molar basis).

X-ray absorption fine structure (XAFS) was recorded at the Cu K edge at room temperature on all the samples in transmission at the XAFS beamline at Elettra, Trieste [38]. Both incident (I0) and transmitted (I) intensities were measured simultaneously using an ionization chamber filled with appropriate gases. Absorber thickness was appropriately adjusted to restrict the absorption edge jump ($\Delta\mu$) to an optimum value. The edge energy was calibrated using Cu metal foil as standard. The as recorded Cu K edge data were reduced following standard procedures in Demeter program [39].

2.3. Test of methanol steam reforming

Before activity measurements, the as prepared catalyst powders were pressed to pellets, then crushed and sieved to 85–100 mesh. The steam reforming of methanol was performed in a continuous-flow quartz micro-reactor (ID = 6 mm) placed in a vertical tube furnace in the temperature range from 200 to 330 °C under atmospheric pressure. The catalyst was packed on a quartz wool bed. The reaction was carried out in step temperature programmed mode by thyristor

controlled Eurotherm PID controller (model 2416), and a K-type thermocouple (Omega) was inserted in the reactor in close contact with the catalyst bed to measure the actual reaction temperature. The pre-mixed methanol (Spectrochem, HPLC grade) and water (Millipore) solution was introduced by a KD100 (Cole Parmer) syringe pump at a rate of 0.6 mL h^{-1}. The liquid mixture was evaporated by heating tapes maintained at 150 °C to ensure a single phase flow. Unless stated otherwise, the reforming experiments in this study were carried out at the steam/methanol (S/M) ratio of 1.1 (molar basis) at a gas hourly space velocity (GHSV) of 30000 h^{-1}.

The analysis of the reaction products was carried out by an online Agilent 7890A gas chromatograph equipped with a thermal conductivity detector (TCD) and a flame ionization detector (FID) and two packed columns (Porapak Q and molecular sieve 5 Å) with argon as the carrier gas. Since methanol was not introduced into the GC, the conversions were calculated by performing a carbon balance.

Methanol conversion (X_{MeOH}) and CO selectivity (S_{CO}) have been calculated by the following equations:

$$X_{MeOH} = \frac{n_{CO2} + n_{CO}}{n_{MeOH}} \times 100 \quad \text{..... (4)}$$

$$S_{CO} = \frac{n_{CO}}{n_{CO2} + n_{CO}} \times 100 \quad \text{..... (5)}$$

where n_{CO} and n_{CO2} are the molar flow rates (mol min^{-1}) of CO and CO_2, respectively, in the dry reformate and n_{MeOH} is the molar flow rate of methanol (mol min^{-1}) in the liquid mixture.

Gas sample from the reactor was analyzed once the system reached the steady state, approximately 50 min after the MSR at a given temperature. At least three gas samples were analyzed for each data point, which gave nearly similar (within 1-2 %) conversion values and the

last GC data were considered as the steady state value. The reproducibility of experimental data was estimated to be within 3%. The equilibrium conversion of methanol and CO selectivity were calculated using the software HSC5.1 (Outokumpu).

MSR was carried out also on samples pretreated in oxidizing (10% O_2 in N_2) or reducing (10% H_2 in N_2) atmosphere. In both cases the catalysts were heated from room temperature to 350 °C at a heating rate of 10 °C min^{-1}, maintained at this temperature for 1 h, cooled to 200 °C in the same atmosphere and finally purged with nitrogen at this temperature followed by switch to MSR gas mixture.

3. Results and Discussion

3.1. Screening of materials for MSR

The MSR activities were tested initially on $Cu_{0.1}Mg_{0.9}Al_2O_4$, $Cu_{0.1}Mn_{0.9}Al_2O_4$, $Cu_{0.1}Fe_{0.9}Al_2O_4$ and $Cu_{0.1}Zn_{0.9}Al_2O_4$. The catalytic activity of copper varies with the A-site cation and it follows the order: Fe> Zn> Mg> Mn (**Figure 1(a)**). The copper ion substituted $FeAl_2O_4$ is the most active formulation exhibiting 98% methanol conversion with a CO selectivity of ~5% at ~300 °C and a GHSV= 30000 h^{-1} (S/M=1.1). The respective methanol conversions were ~60% over $Cu_{0.1}Zn_{0.9}Al_2O_4$, 53% over $Cu_{0.1}Mg_{0.9}Al_2O_4$ and 25% over $Cu_{0.1}Mn_{0.9}Al_2O_4$ under the same reaction conditions.

The methanol conversion and CO selectivity of various copper substituted iron-based spinels ($Cu_xFe_{1-x}Al_2O_4$) are shown in **Figure 1(b)** together with the theoretical equilibrium values. Pure $FeAl_2O_4$ shows almost no activity even at the highest temperature of ~330 °C. About 27% methanol conversion is noted at ~300 °C over the 5 at.% copper substituted sample, CuFeAl5 (not included in the figure). CuFeAl7 shows ~64% methanol conversion with ~4% CO

selectivity at ~300 °C, while CuFeAl10 approaches the equilibrium value at 300 °C and has the maximum conversion at high temperature (**Figure 1(b)**). Further increase in copper loading increases the conversion only up to ~275 °C and is associated with a higher amount of CO formation. The CO selectivity exhibited by all the catalysts lay below the theoretical values in the whole range of temperatures studied. Even though the CO selectivity values remain almost the same between 250 °C and 275 °C for all the catalysts, the methanol conversion increases rapidly. Note that the CO production routes, the methanol decomposition, the reverse water gas shift reaction and the methanol steam reforming reaction are endothermic in nature. Thus these three reactions are kinetically and thermodynamically favored with the increase in temperature. Since the equilibrium conversion is very high, methanol steam reforming is preferred over CO production.

The comparison of the MSR behavior of CuFeAl10 with CuFeAl10IWI shows a much lower methanol conversion (~78% at ~300 °C) over the latter (see **Figure 1(b)**) with similar CO selectivity values, indicating that in the case of the IWI catalyst the CO formation is favored more than over the SCS catalyst.

The differences observed between CuFeAl10 and CuFeAl15 catalysts is likely related with the fact that the increase in the copper loading above 10 at.% results in the formation of CuO clusters, as it appears clearly from the PXRD studies that will be discussed later. From the activity patterns, it can be inferred that the ionically substituted copper in $FeAl_2O_4$ (present in the SCS sample, CuFeAl10) is much more active than the finely dispersed CuO phase (present in the IWI sample, CuFeAl10IWI) for methanol steam reforming.

3.2. Effect of pretreatment, GHSV and S/M ratio

In general, the pretreatment on fresh catalyst can improve the chemical-physical properties of the surface in terms of active phase and its interaction with the support [40, 41]. The effects of oxidizing and reducing pretreatment on CuFeAl10 MSR activity are studied and compared with the fresh CuFeAl10 (without pretreatment). The results are shown in **Figure 2(a)**. The oxidizing pretreatment leads to a methanol conversion almost identical to that of the fresh sample, but a higher amount of CO is formed indicating an increase in CO selectivity. On the contrary, the reducing pretreatment has a negative effect on the MSR behavior, decreasing the conversion significantly and is associated with considerably larger amount of CO formation compared with the fresh catalyst. It is clear then that in the case of SCS catalyst the best catalytic performance is recorded on the fresh sample.

Figure 2(b) shows the MSR behavior at different GHSVs. At GHSV= 10000 h^{-1}, the methanol conversion increases from ~18% at 200 °C to ~85% at 250 °C and complete conversion takes place beyond 275 °C, while the CO selectivity increases beyond 280 °C. At GHSV= 60000 h^{-1}, a maximum of ~86% conversion at 330 °C is reached. Thus CuFeAl10 can tolerate a high space velocity of 60000 h^{-1} preserving high methanol conversion; a similar conversion can be achieved at lower temperature (250 °C) by choosing a lower space velocity (10000 h^{-1}). This behavior can be attributed to the well defined structure of the SCS catalyst: availability of stable lattice sites of the spinel possibly contributes to its considerable catalytic behavior at high space velocity.

The catalytic activity for MSR is influenced also by S/M ratio as shown in **Figure 2(c)** and **(d)**. For S/M= 1, the stoichiometric value, the CO selectivity increases sharply beyond 280 °C approaching the equilibrium value at the highest temperature (**Figure 2(d)**). It is evident that the highest MSR activity can be observed only when a slight excess of water (S/M= 1.1) is used.

With a further increase of S/M ratio the conversion, as well as the CO selectivity, decreases as is usually reported [42].

3.3. Time-on-stream (TOS) MSR behavior

The most common problem associated with the use of copper-based catalysts in methanol reforming is the deactivation by thermal sintering or coke deposition during time-on-stream operation [41, 43]. The TOS reforming behavior of CuFeAl10 and CuFeAl15 is investigated at 250 °C for 20 h with intermediate overnight stay at room temperature in N_2. Both the catalysts exhibit almost similar TOS activity, i.e. the methanol conversion decreases from ~50% after 1 h to ~35% after 20 h of reaction and the CO selectivity of CuFeAl10 is lower than that of CuFeAl15 (**Figure 3)**. The turnover frequencies (TOF) for CuFeAl10 and CuFeAl10IWI catalysts are calculated considering the amount of copper that is present on the catalyst surface obtained from XPS analyses. The CuFeAl10 catalyst shows a higher TOF at 250 °C (1.1 s^{-1}) than CuFeAl10IWI (0.5 s^{-1}). For the aged CuFeAl10, a TOF value of 1.0 s^{-1} is calculated, indicating that the decrease in TOF after ageing is minimal for the combustion synthesized catalyst.

Considering all the standard parameters, Cu-loading, methanol conversion and CO selectivity, it can be concluded that 10 at.% Cu-ion in $FeAl_2O_4$, CuFeAl10, is the best catalyst formulation prepared via the combustion route for MSR.

3.4. BET studies

The surface areas (SAs) of the Cu-based samples are given in **Table 1**. The effect of copper loading is different for the SCS and IWI catalysts. The SA decreases after copper impregnation over the combustion made $FeAl_2O_4$ support (from 129 m^2 g^{-1} for the support [37]

to 89 m^2 g^{-1} for CuFeAl10IWI). On the other side, the one step combustion leads to a SA of about 47 m^2 g^{-1}, lower than the support. This can be attributed to the use of metal nitrate precursors that increase the extent of the exothermic reaction, even if they are present in low amounts [44].

3.5. PXRD studies

The PXRD patterns of the SCS and IWI materials are shown in **Figure 4**. The formation of pure $FeAl_2O_4$ is not evident from PXRD as reported in [37]. The diffraction peaks for spinel phase can be identified only in the presence of copper, and their intensity increases with the increase in copper loading. Thus the formation of $FeAl_2O_4$ phase is facilitated in the presence of copper. All the peaks correspond to $FeAl_2O_4$ spinel phase (JCPDS PDF # 34-0192). No noticeable diffraction due to CuO phase could be distinguished up to the Cu-loading of 10 at.%. The absence of the CuO related peaks suggests that the CuO particles, if formed, are too small to be detected by PXRD or the copper component is substituted as ion in the $FeAl_2O_4$ lattice. Small peaks belonging to CuO (**Figure 4**) appear only in the case of 15 at.% Cu-loaded $FeAl_2O_4$ sample (CuFeAl15), indicating that the $FeAl_2O_4$ phase gets maximum stability with a copper loading of about 10 at. % beyond which the additional copper remains as finely dispersed CuO over the spinel phase. The spinel phase formation is also evident in CuFeAl10IWI catalyst, but the crystallinity is poor in this case when compared with its SCS analogue. Also, the CuO crystal phase could not be detected in its PXRD pattern, suggesting the formation of finely dispersed CuO over the spinel support in the impregnated catalyst. The least-square refined lattice parameters of the $Cu_xFe_{1-x}Al_2O_4$ (x= 0.07-0.15) spinels indicate a systematic decrease, 8.084(5) for 7 at.%, 8.080(5) for 10 at.% to 8.075(2) for 15 at.% copper substituted $FeAl_2O_4$, with the

increase in copper loading. This contraction in lattice parameter is due to the substitution of smaller Cu^{2+} ion (0.57 Å) for Fe^{2+}(0.78 Å) in the $FeAl_2O_4$ lattice.

3.6. TPR studies

The TPR profiles of the various spinels are shown in **Figure 5(a)**. The reducibility behavior strongly depends on the preparation route. The SCS samples show three reduction peaks of which the more pronounced is the one at low temperature (between 190 °C and 350 °C). Interestingly, CuFeAl7 shows a hint of a two stage reduction process which is more evident in CuFeAl10 sample. Due to the higher copper loading in CuFeAl15 that is comprised of both ionically substituted copper and dispersed CuO phase, the peak intensity is comparatively higher and no two step reduction process could be distinguished.

The second peak centered at ~450 °C is a broad one with a much lower intensity, followed by a third small peak in the temperature range 550 °C-700 °C. The second and third peak becomes less intense with the increase of copper loading, CuFeAl15 sample showing an almost negligible third peak.

Unlike the SCS samples, CuFeAl10IWI shows only two strong reduction peaks, with the onset of a third one at high temperature (> 800 °C). The first one is centered at ~290 °C, higher than the low temperature peak position of the SCS samples, while the second broad and intense peak has a maximum at ~625 °C. This is different when compared with the CuFeAl samples prepared via one pot SCS meaning that Cu and Fe have a different interaction on these two samples. The quantitative values obtained from the analyses of the H_2-TPR profiles are listed in the **Table 1** (assuming complete reduction of the nominal amount of copper present in each sample). From a general look at these values, it seems that there is no clear correlation between

the copper loading and the amount of $FeAl_2O_4$ reduction. Probably, since for CuFeAl15 we observe the lowest Fe reduction, we can hypothesize that for lower copper loadings a higher dispersion favors the interaction of Cu with the support and consequently its reduction. Nevertheless this seems in contrast with the fact that for CuFeAl10IWI, the reduction of Fe is completed.

Trying to better understand the TPR profiles and to further characterize the oxidation state of Cu, we carried out PXRD analysis of the samples collected during H_2-TPR, as explained in the experimental section. We focused our attention on the most significant samples, namely CuFeAl10 and CuFeAl10IWI. The diffraction patterns were collected in a Philips X'pert diffractometer (equipped with an X'celerator detector) at 40 kV and 40 mA, using Ni-filtered Cu-Kα radiation in the 2θ range 10°–100° with a step size of 0.02° and a counting time of 80 s per step. **Figure 5(b)** shows a comparison of these PXRD patterns.

Up to 350 °C there are essentially no modifications of the diffraction lines compared to fresh samples; for this reason it is difficult to correlate clearly the low temperature reduction peak to Cu or Fe species. Nevertheless, a slight shift of the spinel characteristic peak to a lower angle might indicate the segregation of some reduced copper out of the original $FeAl_2O_4$ phase.

When the TPR is performed up to 700 °C, the crystallinity of the IWI sample is enhanced dramatically and both the SCS and the IWI patterns become identical. The peaks correspond to the copper-iron spinel phase, but since $CuAl_2O_4$ and $FeAl_2O_4$ have very similar patterns and are only shifted by a very small angle we cannot rule out the simultaneous presence of these two phases. By a careful look at these patterns, the presence of highly dispersed metallic copper could be identified. This result indicates that, up to 700 °C the reductive treatment has similar

effects, even if the TPR profiles are different for CuFeAl10 and CuFeAl10IWI. This might point to different degrees of interaction between Cu and Fe on samples prepared via different routes.

On both the samples reduced up to 1000 °C, the formation of metallic Cu and Fe is clearly distinguished. The main difference between IWI and SCS is that on the first the $FeAl_2O_4$ spinel phase is still there, while on SCS we can observe the formation of aluminum oxide as well as the segregation of iron phase (and/or the formation of a new FeAl reduced phase). Thus, due to the complexity of the spinel system, post TPR X-ray analysis does not give any conclusive insight.

3.7. TEM studies

Figure 6(a) is a general view of CuFeAl10 showing particles of about 5-15 nm in size. **Figure 6(b)** corresponds to a HRTEM image recorded at a higher magnification. The sample contains both well crystallized particles as well as poorly-crystallized ones. Over both types of particles there is always an amorphous, thin shell of material (marked by arrows in **Figure 6(b)**). The Fourier Transform (FT) inset included in **Figure 6(b)** shows rings due to the crystalline particles. Consequently, the rings at 4.70, 2.87, 2.45, 2.02, 1.85, 1.63, 1.56 and 1.43 Å correspond well to copper-iron spinel. In addition, the particles labeled “a” and “b” are monocrystalline domains of copper-iron spinel, according to the spots at 2.87 and 4.70 Å ascribed to (220) and (111) crystallographic planes, respectively. No evidences for the existence of segregated CuO have been encountered by HRTEM. **Figure 6(c)** shows a STEM-HAADF image, where again no segregated phases are identified (note that in STEM-HAADF the segregation of Cu_2O or CuO should appear as bright areas in the image).

Figure 6(d) shows a low-magnification image of the CuFeAl10aged sample, which is constituted by particles of about 10-20 nm indicating some sintering during the MSR reaction. **Figure 6(e)** corresponds to a HRTEM image along with its FT image in which all the lattice fringes identified can be ascribed to the copper-iron spinel. The spots at 2.87 and 2.45 Å are ascribed to (220) and (311) planes of the spinel structure. These values are identical to those recorded over the fresh catalyst, indicating that no structural changes occur under MSR conditions. Also, no copper oxide or metallic copper are identified in the aged sample neither by HRTEM nor STEM-HAADF (**Figure 6(f)**).

Figure 6(g) shows a general view of the CuFeAl15 sample and **Figure 6(h)** corresponds to a HRTEM image. The sample is virtually identical to CuFeAl10. No differences in the lattice fringes of both samples are observed, although they are not expected to vary significantly when increasing the copper content in the spinel structure from 10 to 15 at.%. The size of particles ranges from 5 to 15 nm, as in the case of the CuFeAl10 sample.

The CuFeAl15aged sample is very similar to the CuFeAl10aged sample (**Figure 6(i)**). Again some sintering after MSR is observed; the particles increasing their size up to 10-20 nm. Both well-crystallized and poorly crystallized particles are present (both covered by an amorphous layer, see the areas marked in arrows in **Figure 6(j)**). Again, no evidence for the formation of segregated Cu-containing phases is encountered.

The microstructural findings are strongly supported by PXRD of aged catalysts (**Figure 6(k)**). The spinel phase is retained in the aged samples and no other phase can be detected, indicating that the present spinel catalyst has a very stable structure that does not undergo any decomposition after 20 h of MSR. Interestingly, CuO related peaks detected on CuFeAl15 disappear on ageing. No Cu^0 peak is observed in both the aged samples. This may result from the

reduction of CuO to finely dispersed metallic copper that escaped PXRD analysis. We can thus assume that the substitutional copper ion sites remain mostly intact during ageing. The average crystallite sizes determined from the PXRD data are ~12-13 nm irrespective of the nature of the catalysts, fresh or aged, in close conformity with the TEM analysis.

Figure 6(l) and **6(m)** correspond respectively to a bright field and a HRTEM image of the impregnated spinel sample CuFeAl10IWI. The fresh sample is comprised by particles of 5-15 nm, similar to the SCS samples in their as prepared forms. CuFeAl10IWI also appears to be less crystalline than the SCS samples, in accordance to the PXRD results and in agreement with our previous report on the microstructure of the combustion synthesized pure $FeAl_2O_4$ support [37]. To recall, the general view of $FeAl_2O_4$ is mostly consisted by the flakes of the spinel support that range in size from about 10 to 40 nm. The ring type electron diffraction patterns precisely match with the crystallographic planes of $FeAl_2O_4$ indicating pure spinel phase formation. So, copper impregnation reduces the average crystallite size. However, no other differences between the analogous samples CuFeAl10IWI and CuFeAl10 are evidenced by HRTEM. No CuO particles are detected even in the impregnated sample, which means that the impregnation of copper results in a high dispersion over the $FeAl_2O_4$ spinel support. The absence of segregated CuO particles is corroborated by STEM-HAADF (**Figure 6(n)**).

3.8. XPS studies

In order to have a deeper insight about the surface states of the two types of catalysts, SCS and IWI, we have carried out XPS studies over CuFeAl10 and CuFeAl10IWI samples. The samples are analyzed after *in situ* calcination at 350 °C (the temperature of the muffle furnace used for the synthesis by SCS method; sample names ending with calc350), and after *in situ*

MSR conditions at 300 °C (temperature where the samples are particularly active for MSR under our reaction conditions; sample names ending with MSR300). CuFeAl10 was also analyzed in its as prepared form.

Figure 7(a-f) shows the deconvoluted Cu 2p regions as well as Cu LMM Auger spectra of the CuFeAl10 catalyst. **Table 2** summarizes the relevant data. The as-prepared CuFeAl10 sample exhibits signals of both oxidized copper (Cu^{2+}) and reduced copper (Cu^{1+}), 71% vs. 29%, respectively. After the *in situ* calcination treatment at 350 °C for performing *in situ* MSR experiment, all Cu was oxidized. After MSR, Cu is partially reduced (43%). The shift of the Auger line to lower kinetic energy after MSR with respect to the position of the line after calcination is ascribed to the presence of Cu^{1+} species (**Figure 7 (b, d** and **f)**).

Concerning CuFeAl10IWI, the Cu 2p spectral feature (**Figure 7 (g,i)**) ensures that the calc350 sample is comprised only of oxidized Cu. In the MSR300 sample the reduction of Cu is similar to the CuFeAl10 catalyst (46%; **Table 2**). The Cu LMM Auger spectra (**Figure 7 (h, j)**) also show a contribution at lower kinetic energy in the sample after MSR compared to the calcined catalyst, which is explained by the presence of Cu^{1+} species.

The presence of the reduced copper species Cu^{1+} becomes evident also from the satellite (S) to main $Cu2p_{3/2}$ peak (M) intensity ratio (I_S/I_M). In CuO, this ratio is 0.55 [45]. For CuFeAl10, the intensity ratios are 0.31, 0.55 and 0.24, respectively, for its as prepared, calc350 and MSR300 forms. So, both the as prepared and MSR treated samples exhibit a lower I_S/I_M ratio compared to the *in situ* calcined sample. This indicates the presence of reduced Cu^{1+} species in the first two forms of the catalyst. The I_S/I_M ratio exhibits a much larger value of 1.07 for CuFeAl10 calc350. Nevertheless, in MSR environment a surface characteristics similar to that of the SCS catalyst is obtained (I_S/I_M= 0.23).

The dispersion of Cu in the as prepared sample by SCS method and by IWI method is similar. The Cu/(Fe+Al) ratio of as prepared CuFeAl10 sample is 7.1%, which is in accordance to the Cu-loading of 10 at.%. The Cu/(Fe+Al) ratios of samples CuFeAl10 and CuFeAl10IWI after calcination are 7.6% and 9.4%, respectively, whereas after MSR they are 5.8% and 6.3%, respectively. This lowering of surface concentration of copper is probably due to sintering of the spinel crystal phases under MSR conditions.

The Fe species do not seem to undergo appreciable transformation under MSR as appears from the respective BE values in the 2p spectra that suggest presence of Fe^{2+} (**Table 2**). Nevertheless, from the above analysis of Cu oxidation state the presence of a minor amount of Fe^{3+} together with Fe^{2+} cannot be completely ruled out. Aluminum maintains its robust oxidation state of 3+ as confirmed from its BE value in all the samples (**Table 2**).

From XPS measurements over CuFeAl10 it results that only a part of surface copper is reduced under MSR conditions. The fact that XPS reveals the presence of surface reduced copper but HRTEM does not identify any segregated Cu, Cu_2O or CuO phase is an indication that reduction of copper under MSR is restricted at the surface of the spinel particles. This is also in accordance to the observation that the atomic surface Cu/Al ratio before and after the reforming reaction (0.10-0.11 vs. 0.08) decreases only slightly.

The microstructural findings on CuFeAl10IWI are in accordance to the XPS characterization of the as prepared sample, where the Cu/Al atomic surface composition was fairly similar or even higher (Cu/Al= 0.14 for the calc350 sample and 0.09 for the MSR300 sample) than that of the CuFeAl10 catalyst (0.14 vs. 0.10-0.11, respectively). Therefore, TEM and XPS do not point out to strong differences between CuFeAl10 and CuFeAl10IWI.

3.9. XANES studies

In **Figure 8(a)** Cu K edge XANES in Cu metal, Cu_2O and CuO are presented along with those in CuFeAl10 and CuFeAl10aged catalysts. A clear shift to lower energies can be seen in the position of the Cu K edge in the aged sample. Though this shift is much less compared to that between CuO and Cu_2O or Cu metal XANES spectra, it indicates the presence of Cu reduced species along with Cu^{2+} in CuFeAl10aged. Together with the edge shift, a growth of a new feature on the lower energy side of the main resonance peak is also detected in the XANES of CuFeAl10aged. The energy position of this feature compares better with the main resonance peak of Cu_2O rather than that of Cu metal suggesting the presence of Cu^{1+} along with Cu^{2+} in the aged sample, according to XPS studies. The Cu K edge XANES in CuFeAl15 and CuFeAl15aged samples (not shown) are exactly similar to the respective as prepared and aged samples of CuFeAl10. In the case of CuFeAl10IWI, the Cu K XANES indicates the presence of only Cu^{2+} and agrees with the literature reports [27, 29].

The presence of Cu^{1+} on SCS sample becomes more evident in the derivative spectra of Cu K edge shown in **Figure 8(b)**. The spectrum of the as prepared CuFeAl10 shows its first maxima at about 8986 eV. In the aged sample, another maximum appears as a shoulder peak at 3.5 eV below the peak at 8986 eV. If one compares the derivative spectra of the Cu K absorption edge in Cu metal, Cu_2O and CuO presented in **Figure 8(c)**, the energy difference between the first maxima of Cu metal and Cu_2O with respect to that of CuO is 5.1 eV and 3.4 eV, respectively. This observation again points to the presence of Cu^{1+} species in CuFeAl10aged. Interestingly, the presence of this Cu^{1+} species can also be noted in the as prepared sample from the shoulder in its derivative spectrum (**Figure 8(b)**), even if in lower amount.

In summary, the experimental findings indicate that the copper phase(s) dispersed in $FeAl_2O_4$ spinel by the SCS and IWI methods are of different nature. CuFeAl10IWI contains tiny CuO crystallites (size being below the detection limit of TEM), whereas on CuFeAl10 the oxidized copper is present as substitutional Cu ions in the $FeAl_2O_4$ spinel. This structural difference between the two materials (SCS vs. IWI) with different types of copper ionic species (substitutional Cu^{2+} ion vs. CuO) is the main cause for the higher MSR activity of the combustion made catalyst, even with lower surface area. The well-defined structure of CuFeAl10 containing lattice Cu-ion sites seems thus to be the major responsible for the higher MSR activity of SCS catalyst. In fact, also the Cu^{2+}/Cu^{1+} ratio is not very much different between CuFeAl10 and CuFeAl10IWI in their various forms (**Table 2**). Moreover, the presence of Cu^{1+} species is also evident in the aged sample from XANES analysis. The loss in MSR activity during TOS tests recorded for the SCS catalysts can be attributed to the sintering of catalyst crystallites (from 5-15 nm in the as prepared samples to 10-20 nm in the aged samples as observed by HRTEM analysis) with concomitant decrease of surface copper concentration.

A direct comparison of the spinel based MSR catalysts reported in the literature with our present spinel catalyst is not straight forward as the spinels are different and there are many differences in the experimental conditions as well. Majority of the available Cu-spinel materials are pure spinels Cu-Mn [19, 32], Cu-Fe [19], Cu-Al [24] and Cu-X (X= Mn, Fe, Al and La) [33]. Other catalysts are the mixed oxides of Cu-Mn spinel and Mn-oxide [25-27]; supported spinels like Cu-Fe on silica [28] and SBA-15 [29]; Cu-Al spinel (together with slight excess of CuO) on pseudobohemite [31]; and Cu-loaded Zn-Al spinel [30, 35]. In general, many of these systems exhibit high MSR activity despite their low SA ($< 10\ m^2\ g^{-1}$), but undergo phase decomposition.

Most of these spinel catalysts require a reductive pretreatment, even if in some cases, an oxidative pretreatment resulted in good MSR activity [25, 26].

By far the best MSR behavior is exhibited by the $CuAl_2O_4$ catalyst when it contains a little excess of CuO, but it requires a high pressure of 1.0 MPa [31]. The Cu-Mn spinel is a very efficient MSR catalyst after an oxidative pretreatment showing 99.3% conversion with 3.1% CO selectivity at 240 °C and S/M= 1.5 [26]. Time-on-stream (8 h) activity of this catalyst shows a minimal decrease in conversion [25]. The reduced Cu-Mn spinel catalyst exhibits complete methanol conversion at a high temperature of 371 °C and low GHSV (wet base) of 2000 h^{-1} [27]. High surface area Cu-Mn spinel also showed high MSR performance at a very high WHSV of 27.2 h^{-1} [32]. The $CuFe_2O_4/SiO_2$ catalyst also exhibits high MSR activity at a high temperature of 360 °C [28]. High surface area $CuFe_2O_4$ synthesized using mesoporous silica as the template gives 100% methanol conversion at 240 °C probably due to the formation of nano-sized copper after hydrogen reduction at 300 °C at a WHSV lower than our MSR tests (1.24 h^{-1} vs. 3.2 h^{-1}) [29]. Study on the CuX_2O_4 (X= Mn, Fe, Al and La) systems shows $CuAl_2O_4$ as the best one exhibiting the TOF of 327.6 s^{-1} at 280 °C and LHSV= 25 h^{-1} [33]. When 20 wt.% copper is dispersed on $ZnAl_2O_4$ support, 100% methanol conversion is achieved at 200 °C with a TOF of 0.73 min^{-1} at 200 °C at GHSV= 2400 h^{-1} [30]. The copper substituted $ZnAl_2O_4$ is an effective precursor for thermally stable Cu catalysts showing ~98% methanol conversion at 260 °C up to 20 h [35]. Other Cu-Mn and Cu-Fe spinels are reported to have methanol conversions of ~88% and ~94% respectively at 300 °C and GHSV of 24000 h^{-1} [19].

In **Table 3** the activity behavior of CuFeAl10 is compared with a few benchmark catalytic systems in order to better judge its performances and it turns out that its activity is comparable [13] or higher [19] with respect to the materials considered.

Only a few studies report the effects of ionic substitution of the first row transition metal ions in the parent spinel lattice. Huang et al. have shown that the substitution of Ni into $CuFe_2O_4$ ($Ni_{0.5}Cu_{0.5}Fe_2O_4$) is effective for MSR, but the spinel phase decomposes after H_2 treatment and the catalyst suffers from a very high CO selectivity (~70%) as well as CH_4 production [34]. Also $Cu_{1-x}Zn_xAl_2O_4$ with interesting microstructural features works very well for MSR [35]. The easily made combustion synthesized catalyst CuFeAl10 reported in this study containing substitutional Cu-ion sites in the spinel lattice exhibits ~98% conversion at 300 °C with a CO selectivity of ~5% which is a very promising result when compared with the literature reports as discussed above. In particular, compared to other systems CuFeAl10 (i) is formed in about a minute and does not require any pretreatment; (ii) contains just 10 at.% Cu (3.6 wt.%; by far the lowest loading) being fairly active for MSR; and (iii) does not undergo phase decomposition even after the ageing treatment indicating high stability of the Cu-ion substituted $FeAl_2O_4$ spinel catalyst. The activity decrease of CuFeAl10 with TOS is due to the sintering of catalyst crystallites in the MSR atmosphere. Despite this, CuFeAl10 maintains a methanol conversion of 35% at 250 °C after 20 h of reaction at GHSV= 30000 h^{-1}. In order to get a larger methanol conversion under the same set of experimental conditions, it is necessary to perform the reaction at a lower space velocity as demonstrated in our study. These findings on the synthesis of copper ion substituted $FeAl_2O_4$ spinel system showing interesting MSR behavior are expected to pave the way for the development of stable single phase Cu-spinel based catalysts with a low copper loading.

4. Conclusions

We have fruitfully demonstrated a single step solution combustion synthesis as a very easy and fast method for the preparation of single phase $Cu_{0.1}Fe_{0.9}Al_2O_4$ spinel that is a suitable catalyst for the methanol steam reforming reaction achieving 98% conversion at 300 °C and GHSV= 30000 h^{-1} using a S/M ratio of 1.1 (molar basis). The PXRD analyses as well as HRTEM investigations have revealed the formation of a very stable spinel phase containing substitutional copper ions that remain intact even after the 20 h of reaction. Moreover, the combustion synthesized sample is superior to its impregnated analogue despite its lower surface area because of the higher crystallinity of the former that makes available the active ionic copper species in a more efficient manner than the latter sample. The loss of activity of combustion synthesized catalyst during time-on-stream tests is likely originated from the sintering of catalyst crystallites that has the effect of lowering the surface concentration of copper. Finally, the solution combustion synthesis route offers great advantages with respect to the preparation and potential applicability in heterogeneous catalysis.

Acknowledgements

Financial supports from the Department of Science and Technology, Government of India, by a grant (SR/S1/PC-28/2010) to AG and research fellowship to SM and DST Special Grant to the Department of Chemistry of Jadavpur University in the International Year of Chemistry 2011 are gratefully acknowledged. JLl is Serra Húnter Fellow and is grateful to ICREA Academia program (Generalitat de Catalunya). SC and AT acknowledges funding from Italian Ministry under FIRB project RBFR10S4OW and JLl and MD acknowledge funding from Spanish Ministry under MINECO project ENE2012-36368.

References

[1] J.M. King, M.J. O'Day, Applying fuel cell experience to sustainable power products, J. Power Sources 86 (2000) 16–22.

[2] D. Ramirez, L.F. Beites, F. Blazquez, J.C. Ballesteros, Distributed generation system with PEM fuel cell for electrical power quality improvement, Int. J. Hydrogen Energy 33 (2008) 4433–4443.

[3] Y. Choi, H.G. Stenger, Fuel cell grade hydrogen from methanol on a commercial $Cu/ZnO/Al_2O_3$ catalyst, Appl. Catal. B: Environ. 38 (2002) 259–269.

[4] B. Lindström, L.J. Pettersson, Hydrogen generation by steam reforming of methanol over copper-based catalysts for fuel cell applications, Int. J. Hydrogen Energy 26 (2001) 923–933.

[5] S.D. Jones, H.E. Hagelin-Weaver, Steam reforming of methanol over CeO_2- and ZrO_2-promoted Cu-ZnO catalysts supported on nanoparticle Al_2O_3, Appl Catal B: Environ. 90 (2009) 195–204.

[6] D. Srinivas, C.V.V. Satyanarayana, H.S. Potdar, P. Ratnasamy, Structural studies on NiO-CeO_2-ZrO_2 catalysts for steam reforming of ethanol, Appl. Catal. A: Gen. 246 (2003) 323–334.

[7] K. Tekeishi, H. Suzuki, Steam reforming of dimethyl ether, Appl. Catal. A: Gen. 260 (2004) 111–117.

[8] K.O. Rocha, J.B.O. Santos, D. Meira, P.S. Pizani, C.M.P. Marques, D. Zanchet, J.M.C. Bueno, Catalytic partial oxidation and steam reforming of methane on La_2O_3–Al_2O_3 supported Pt catalysts as observed by X-ray absorption spectroscopy, Appl. Catal. A: Gen. 431 (2012) 79–87.

[9] G.W. Huber, J.W. Shabaker, S.T. Evans, J.A. Dumesic, Aqueous-phase reforming of ethylene glycol over supported Pt and Pd bimetallic catalysts, Appl. Catal. B: Environ. 62 (2006) 226–235.

[10] J. Agrell, M. Boutonnet, J.L.G. Fierro, Production of hydrogen from methanol over binary Cu/ZnO catalysts, Part II. Catalytic activity and reaction pathways, Appl. Catal. A: Gen. 253 (2003) 213–223.

[11] K. Kumabe, S. Fujimoto, T. Yanagida, M. Ogata, T. Fukuda, A. Yabe, T. Minowa, Environmental and economic analysis of methanol production process via biomass gasification, Fuel 87 (2008) 1422–1427.

[12] B.A. Peppley, J.C. Amphlett, L.M. Kearns, R.F. Mann, Methanol–steam reforming on $Cu/ZnO/Al_2O_3$. Part 1: the reaction network, Appl. Catal. A: Gen. 179 (1999) 21–29.

[13] S.D. Jones, L.M. Neal, H.E. Hagelin-Weaver, Steam reforming of methanol using Cu-ZnO catalysts supported on nanoparticle alumina, Catal. B: Environ. 84 (2008) 631–642.

[14] L. Gama, M.A. Ribeiro, B.S. Barros, R.H.A. Kiminami, I.T. Weber, A.C.F.M. Costa, Synthesis and characterization of the $NiAl_2O_4$, $CoAl_2O_4$ and $ZnAl_2O_4$ spinels by the polymeric precursors method, J Alloys. Compd. 483 (2009) 453–455.

[15] Y. Tanaka, T. Ukata, R. Kikuchi, T. Takeguchi, K. Sasaki, K. Eguchi, Water gas shift reaction for the reformed fuels over Cu/MnO catalysts prepared via spinel-type oxide, J. Catal. 215 (2003) 271–278.

[16] F. Severino, J.L. Brito, J. Laine, J.L.G. Fierro, A. L. Agudo, Nature of copper active sites in the carbon monoxide oxidation on $CuAl_2O_4$ and $CuCr_2O_4$ spinel type catalysts, J. Catal. 177 (1998) 82–95.

[17] A.H. de M. Batista, F.S.O. Ramos, T.P. Braga, C.L. Lima, F.F. de Sousa, E.B.D. Barros, J. M. Filho, A.S. de Oliveira, J.R. de Sousa, A. Valentini, A.C. Oliveira, Mesoporous MAl_2O_4 (M= Cu, Ni, Fe or Mg) spinels: Characterization and application in the catalytic dehydrogenation of ethylbenzene in the presence of CO_2, Appl. Catal. A: Gen. 382 (2010) 148–157.

[18] K. Faungnawakij, N. Shimoda, T. Fukunaga, R. Kikuchi, K. Eguchi, Cu-based spinel catalysts CuB_2O_4 (B = Fe, Mn, Cr, Ga, Al, $Fe_{0.75}Mn_{0.25}$) for steam reforming of dimethyl ether, Appl. Catal. A: Gen. 341 (2008) 139–145.

[19] Y. Tanaka, R. Kikuchi, T. Takeguchi, K. Eguchi, Steam reforming of dimethyl ether over composite catalysts of γ-Al2O3 and Cu-based spinel, Appl. Catal. B: Environ. 57 (2005) 211–222.

[20] K. Faungnawakij, R. Kikuchi, T. Fukunaga, K. Eguchi, Stability enhancement in Ni-promoted Cu-Fe spinel catalysts for dimethyl ether steam reforming, J. Phys. Chem. C 113 (2009) 18455–18458.

[21] M.N. Barroso, M.F. Gomez, L.A. Arrua, M.C. Abello, Reactivity of aluminum spinels in the ethanol steam reforming reaction, Catal. Lett. 109 (2006) 13–19.

[22] H. Muroyama, R. Nakase, T. Matsui, K. Eguchi, Ethanol steam reforming over Ni-based spinel oxide, Int. J. Hydrogen Energy 35 (2010) 1575–1581.

[23] F. Aupretre, C. Descorme, D. Duprez, D. Casanave, D. Uzio, Ethanol steam reforming over $Mg_xNi_{1-x}Al_2O_3$ spinel oxide-supported Rh catalysts, J. Catal. 233 (2005) 464–477.

[24] M. Matsukata, S. Uemiya, E. Kikuchi, Copper-alumina spinel catalysts for steam reforming of methanol, Chem. Lett. (1988) 761–764.

[25] J. Papavasiliou, G. Avgouropoulos, T. Ioannides, Combined steam reforming of methanol over Cu–Mn spinel oxide catalysts, J. Catal. 251 (2007) 7–20.

[26] J. Papavasiliou, G. Avgouropoulos, T. Ioannides, Steam reforming of methanol over copper–manganese spinel oxide catalysts, Catal. Commun. 6 (2005) 497–501.

[27] T. Fukunaga, N. Ryumon, N. Ichikuni, S. Shimazu, Characterization of CuMn-spinel catalyst for methanol steam reforming, Catal. Commun. 10 (2009) 1800–1803.

[28] S. Kameoka, T. Tanabe, A.P. Tsai, Spinel $CuFe_2O_4$: a precursor for copper catalyst with high thermal stability and activity, Cat. Lett. 100 (2005) 89–93.

[29] S.C. Yang, W.N. Su, S.D. Lin, J. Rick, J.H. Cheng, J.Y. Liu, C.J. Pan, D.G. Liu, J.F. Lee, T.S. Chan, H.S Sheu, B.J. Hwang, Preparation of nano-sized Cu from a rod-like $CuFe_2O_4$: suitable for high performance catalytic applications, Appl. Catal. B: Environ. 106 (2011) 650–656.

[30] P. Mierczynski, K. Vasilev, A. Mierczynska, W. Maniukiewicz, T. Maniecki, The effect of $ZnAl_2O_4$ on the performance of $Cu/Zn_xAl_yO_{x+1.5y}$ supported catalysts in steam reforming of methanol, Top. Catal. 56 (2013) 1015–1025.

[31] H. Xi, X. Hou, Y. Liu, S. Qing, Z. Gao, Cu–Al spinel oxide as an efficient catalyst for methanol steam reforming, Angew. Chem. Int. Ed. 53 (2014) 11886–11889.

[32] G. Marbán, T.V. Solis, A.B. Fuertes, High surface area $CuMn_2O_4$ prepared by silica-aquagel confined co-precipitation: Characterization and testing in steam reforming of methanol (SRM), Catal. Lett. 118 (2007) 8–14.

[33] Y.H. Huang, S.F. Wang, A.P. Tsai, S. Kameoka, Reduction behaviors and catalytic properties for methanol steam reforming of Cu-based spinel compounds CuX_2O_4 (X=Fe, Mn,Al,La), Ceram. Int. 40 (2014) 4541–4551.

[34] Y.H. Huang, S.F. Wang, A.P. Tsai, S. Kameoka, Catalysts prepared from copper–nickel ferrites for the steam reforming of methanol, J. Power Sources 281 (2015) 138–145.

[35] F. Conrad, C. Massue, S. Kühl, E. Kunkes, F. Girgsdies, I. Kasatkin, B. Zhang, M. Friedrich, Y. Luo, M. Armbrüster, G.R. Patzke, M. Behrens, Microwave-hydrothermal synthesis and characterization of nanostructured copper substituted ZnM_2O_4 (M= Al, Ga) spinels as precursors for thermally stable Cu catalysts, Nanoscale 4 (2012) 2018–2028.

[36] S.T. Yong, C.W. Ooi, S.P. Chai, X.S. Wu, Review of methanol reforming-Cu-based catalysts, surface reaction mechanisms and reaction schemes, Int. J. Hydrogen Energy 38 (2013) 9541–9552.

[37] R. Mistri, S. Maiti, J. Llorca, M. Dominguez, T. K. Mandal, P. Mohanty, B. C. Ray, A. Gayen, Copper ion substituted hercynite ($Cu_{0.03}Fe_{0.97}Al_2O_4$): A highly active catalyst for liquid phase oxidation of cyclohexane, Appl. Catal. A: Gen. 485 (2014) 40–50.

[38] A. D. Cicco, G. Aquilanti, M. Minicucci, E. Principi, N. Novello, A. Cognigni, L. Olivi, Novel XAFS capabilities at ELETTRA synchrotron light source, J. Phys. Conf. Ser. 190 (2009) 012043.

[39] B. Ravel, M. Newville, ATHENA, ARTEMIS, HEPHAESTUS: data analysis for X-ray absorption spectroscopy using IFEFFIT, J. Synchrotron Radiat. 12 (2005) 537–541.

[40] M. Mavrikakis, P. Stoltze, J.K. Nørskov, Making gold less noble, Catal. Lett. 64 (2000) 101–106.

[41] C. Pojanavaraphan, A. Luengnaruemitchai, E. Gulari, Catalytic activity of Au-Cu/CeO_2-ZrO_2 catalysts in steam reforming of methanol, Appl. Catal. A: Gen. 456 (2013) 135–143.

[42] S. Patel, K.K. Pant, Activity and stability enhancement of copper–alumina catalysts using cerium and zinc promoters for the selective production of hydrogen via steam reforming of methanol, J. Power Sources 159 (2006) 139–143.

[43] M.V. Twigg, M.S. Spencer, Deactivation of copper metal catalysts for methanol decomposition, methanol steam reforming and methanol synthesis, Top. Catal. 22 (2003) 191–203.

[44] S. Colussi, A. Gayen, M. Boaro, J. Llorca, A. Trovarelli, Influence of different palladium precursors on the properties of solution-combustion-synthesized palladium/ceria catalysts for methane combustion, Chem. Cat. Chem. 7 (2015) 2222–2229.

[45] Y. Okamoto, K. Fukino, T. Imanaka, S. Teranishi, Surface characterization of copper(II) oxide-zinc oxide methanol-synthesis catalysts by x-ray photoelectron spectroscopy. 1. Precursor and calcined catalysts, J. Phys. Chem. 87 (1983) 3740–3747.

Table 1: Nominal composition, name, textural and redox (quantitative analysis of TPR data) properties of the copper spinel catalysts

Nominal composition	**Name**	**Nominal Cu wt.%**	**Surface area (m^2 g^{-1})**	**Pore volume (cm^3 g^{-1})**	**Pore size (Å)**
$Cu_{0.07}Fe_{0.93}Al_2O_4$	CuFeAl7	2.55	46.7	0.358	196
$Cu_{0.10}Fe_{0.90}Al_2O_4$	CuFeAl10	3.64	48.3	0.329	183
$Cu_{0.15}Fe_{0.85}Al_2O_4$	CuFeAl15	5.45	47.6	0.340	206
CuO (10 at.%)/$FeAl_2O_4$	CuFeAl10IWI	3.64	89.3	0.469	185

Table 2: XPS data of CuFeAl10 and CuFeAl10IWI samples

Sample	**Name**	**Position (eV)**	**Element**	**% At Conc**	**%Cu (Cu^0, Cu^+)**	**%Cu (Cu^{2+})**
CuFeAl10 calc350	Fe $2p_{3/2}$	710.6	Fe	27.5		
	Cu 2p3/2	932.9	Cu	7.1	0	100
	Al $2p_{3/2}$	74.7	Al	65.4		
CuFeAl10 MSR300	Fe $2p_{3/2}$	709.6	Fe	26.6		
	Cu 2p3/2	931.0	Cu	5.5	43	57
	Al $2p_{3/2}$	72.9	Al	67.9		
CuFeAl10IWI calc350	Fe $2p_{3/2}$	710.4	Fe	27.8		
	Cu 2p3/2	933.9	Cu	8.6	0	100
	Al $2p_{3/2}$	74.9	Al	63.6		
CuFeAl10IWI MSR300	Fe $2p_{3/2}$	709.0	Fe	26.7		
	Cu 2p3/2	930.9	Cu	5.9	46	54
	Al $2p_{3/2}$	73.0	Al	67.4		

List of Figures

Figure 1: The MSR behavior of (a) various combustion synthesized 10 at. % copper loaded spinels and (b) effects of copper loading via solution combustion in $FeAl_2O_4$ spinel at GHSV of 30000 h^{-1} (S/M= 1.1; balance is N_2 in each case).

Figure 2: The MSR behavior of CuFeAl10 (a) under different pretreatment conditions (S/M= 1.1), (b) as a function of GHSV (S/M= 1.1) and (c) as a function of S/M molar ratio at GHSV of 30000 h^{-1} (balance is N_2 in each case).

Figure 3: The time on stream MSR activity patterns at 250 °C of CuFeAl10 and CuFeAl15 catalysts at GHSV of 30000 h^{-1} (balance is N_2 in each case).

Figure 4: The H_2-TPR profiles of various (combustion synthesized and impregnated) copper loaded $FeAl_2O_4$ spinel oxides.

Figure 5: The PXD patterns of pure and various copper loaded spinel oxides.

Figure 6: TEM images of (a-c) CuFeAl10, (d-f) CuFeAl10aged (g, h) CuFeAl15, (i, j) CuFeAl15aged and (l-n) CuFeAl10IWI; (k) represents the slow scan PXD data of CuFeAl10 and CuFeAl15 in their as prepared and aged forms in the 2θ range 25–50 degrees.

Figure 7: XPS of Cu 2p region and Cu LMM Auger spectra of (a, b) as-prepared, (c, d) calc350 and (e, f) MSR300 samples of CuFeAl10.

Figure 8: XPS of Cu 2p region and Cu LMM Auger spectra of (a, b) calc350 and (c, d) MSR300 samples of CuFeAl10IWI.

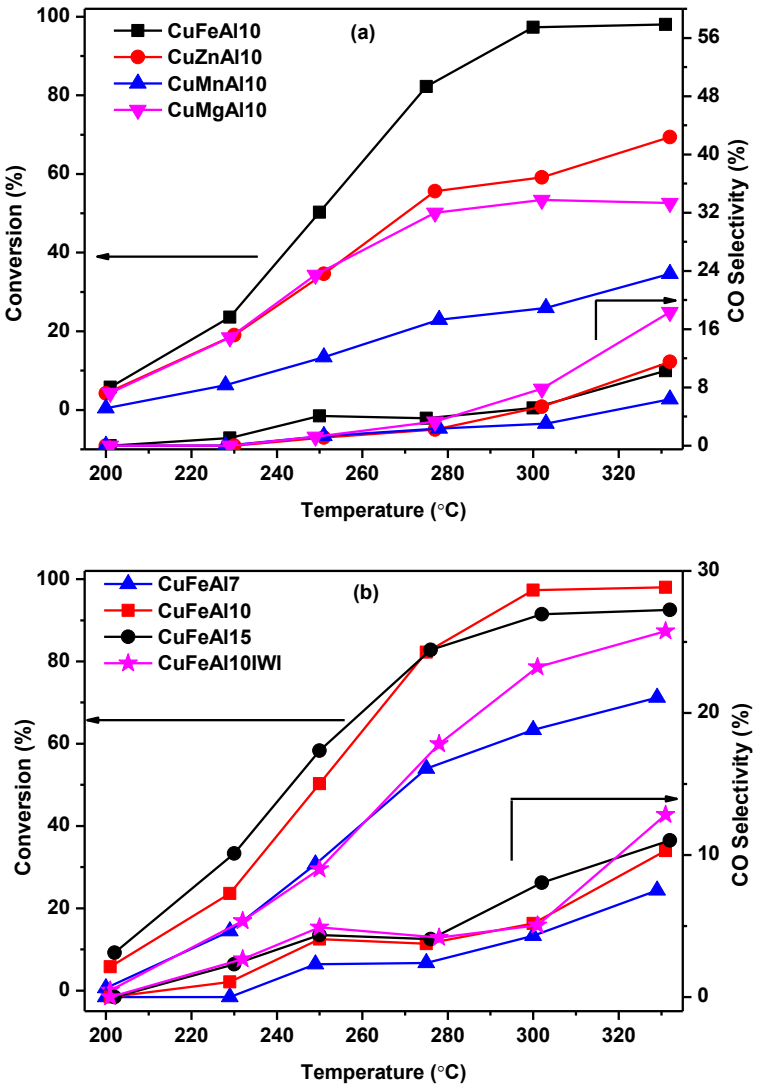
(a)
CuFeAl10
CuZnAl10
CuMnAl10
CuMgAl10
Conversion (%)
CO Selectivity (%)
Temperature (°C)
(b)
CuFeAl7
CuFeAl10
CuFeAl15
CuFeAl10IWI
Conversion (%)
CO Selectivity (%)
Temperature (°C)

Fig. 1

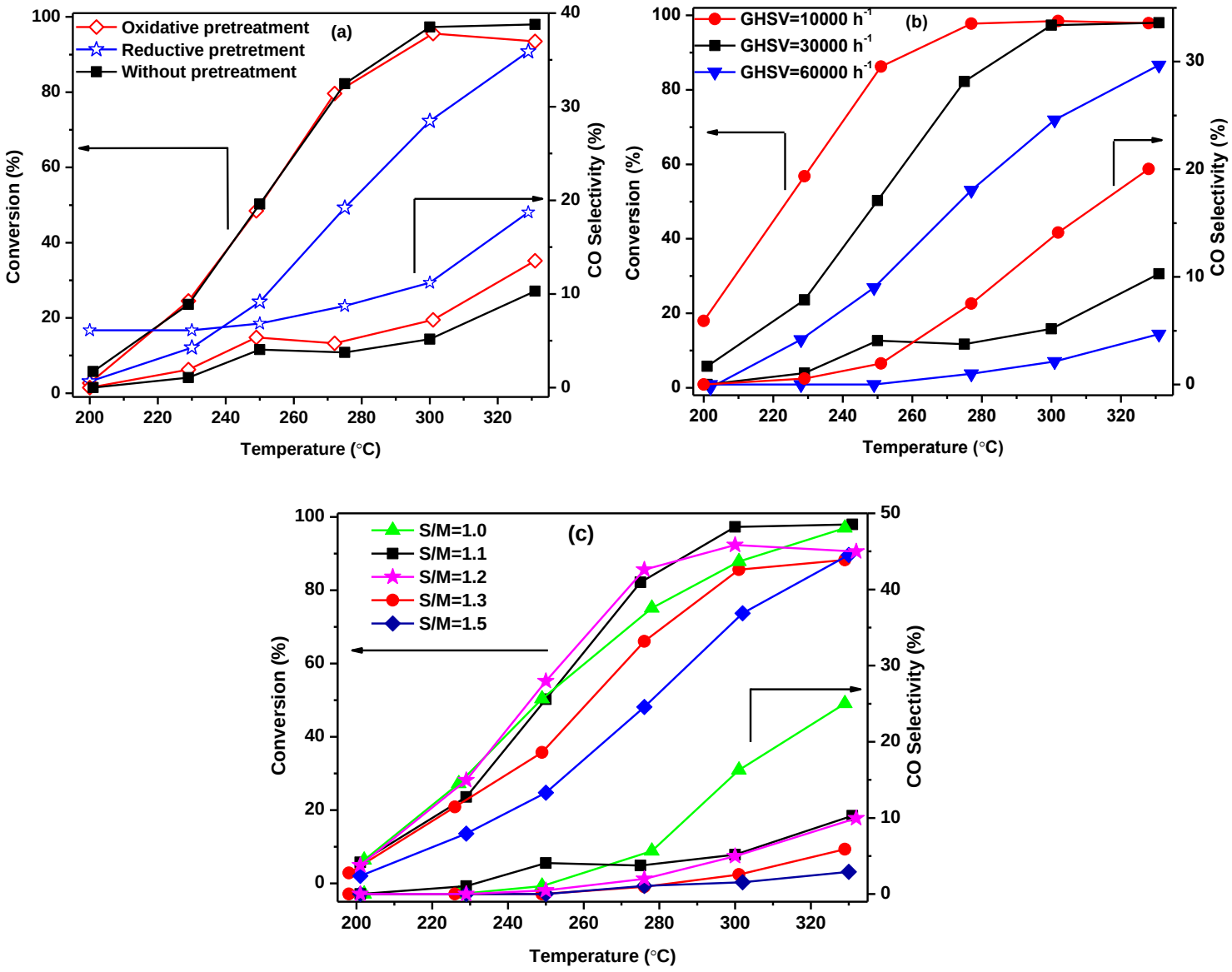
(a)
Oxidative pretreatment
Reductive pretretment
Without pretreatment
Conversion (%)
CO Selectivity (%)
Temperature (°C)
(b)
GHSV=10000 h-1
GHSV=30000 h-1
GHSV=60000 h-1
Conversion (%)
CO Selectivity (%)
Temperature (°C)
(c)
S/M=1.0
S/M=1.1
S/M=1.2
S/M=1.3
S/M=1.5
Conversion (%)
CO Selectivity (%)
Temperature (°C)

Fig. 2

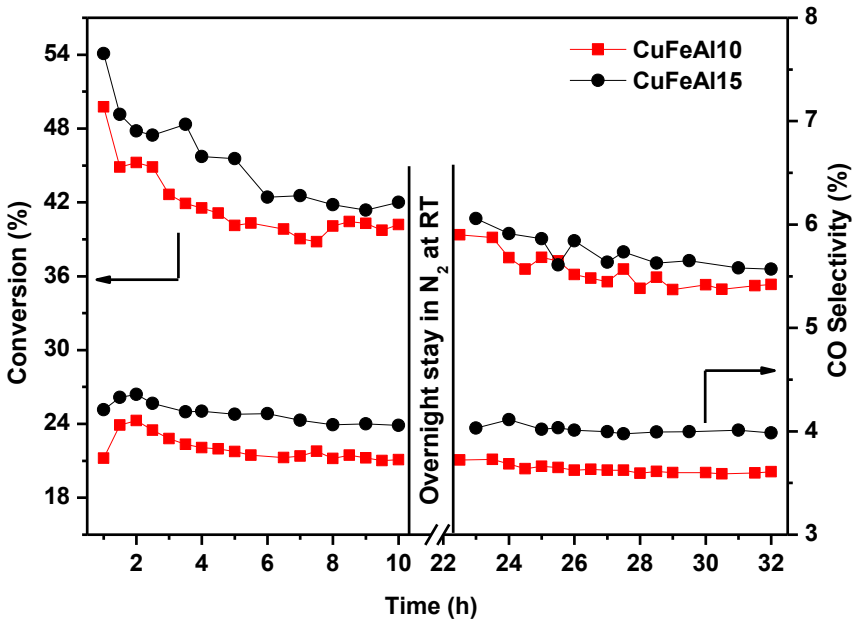
CuFeAl10
CuFeAl15
Conversion (%)
CO Selectivity (%)
Overnight stay in N2 at RT
Time (h)
54
48
42
36
30
24
18
8
7
6
5
4
3
2
4
6
8
10
22
24
26
28
30
32

Fig. 3

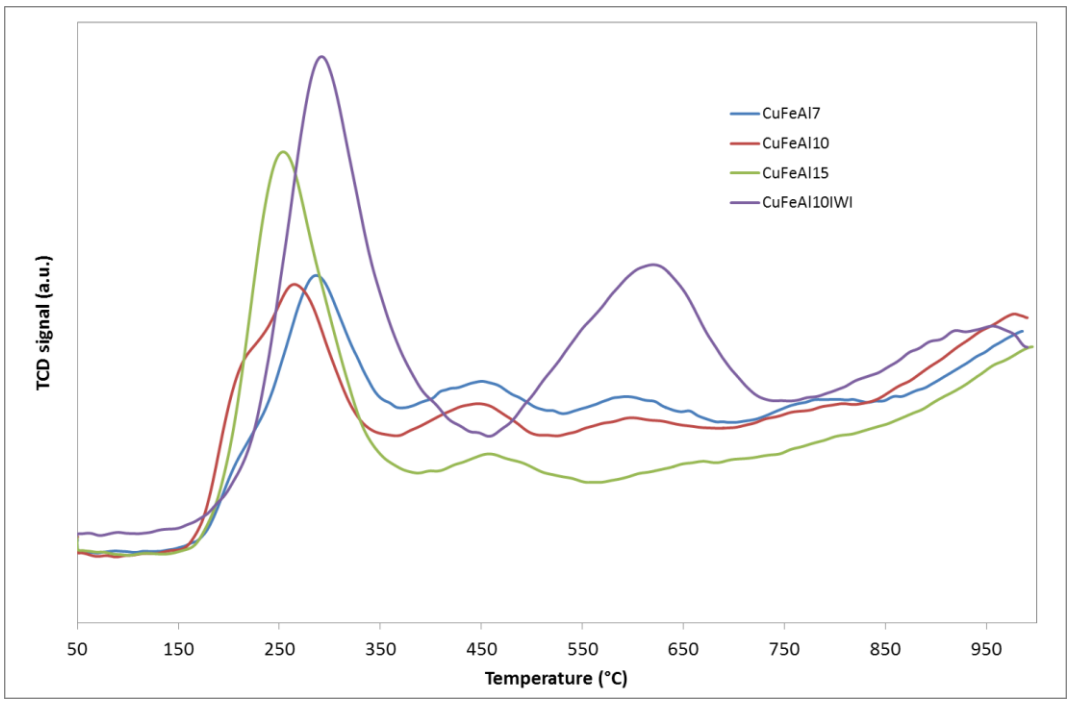
CuFeAl7
CuFeAl10
CuFeAl15
CuFeAl10IWI
TCD signal (a.u.)
Temperature (°C)
50
150
250
350
450
550
650
750
850
950

Fig. 4

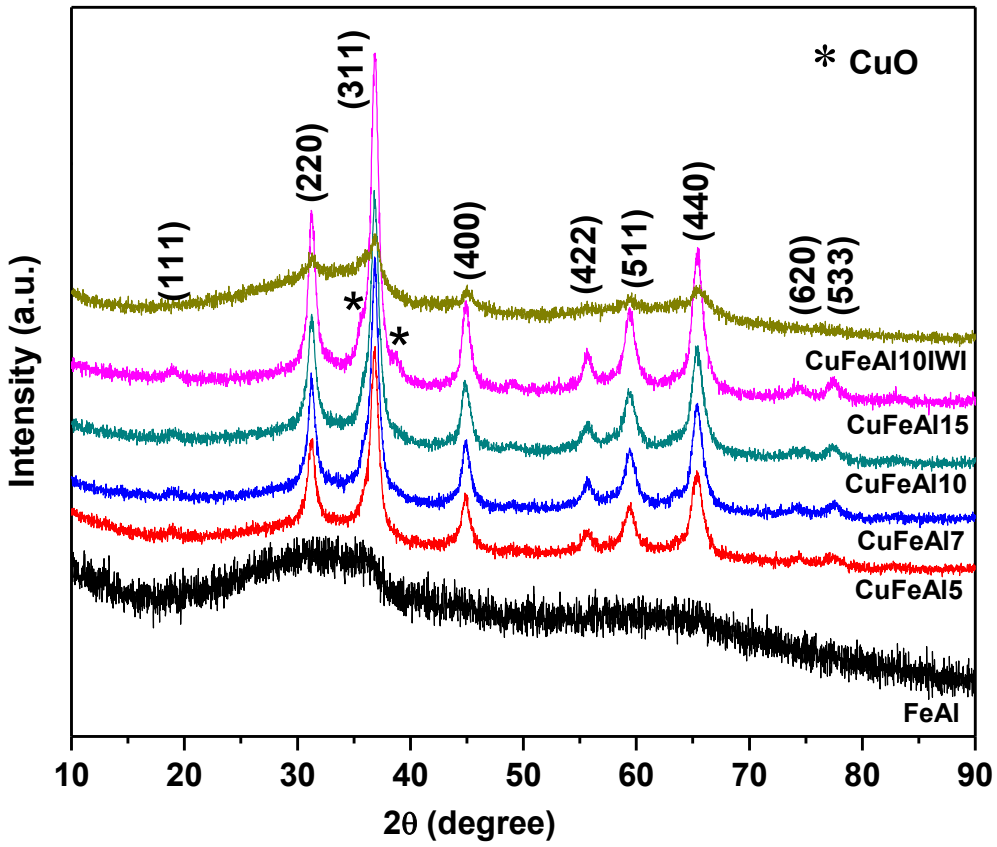
* CuO
(111)
(220)
(311)
(400)
(422)
(511)
(440)
(620)
(533)
*
*
CuFeAl10lWl
CuFeAl15
CuFeAl10
CuFeAl7
CuFeAl5
FeAl
Intensity (a.u.)
10
20
30
40
50
60
70
80
90
2θ (degree)

Fig. 5

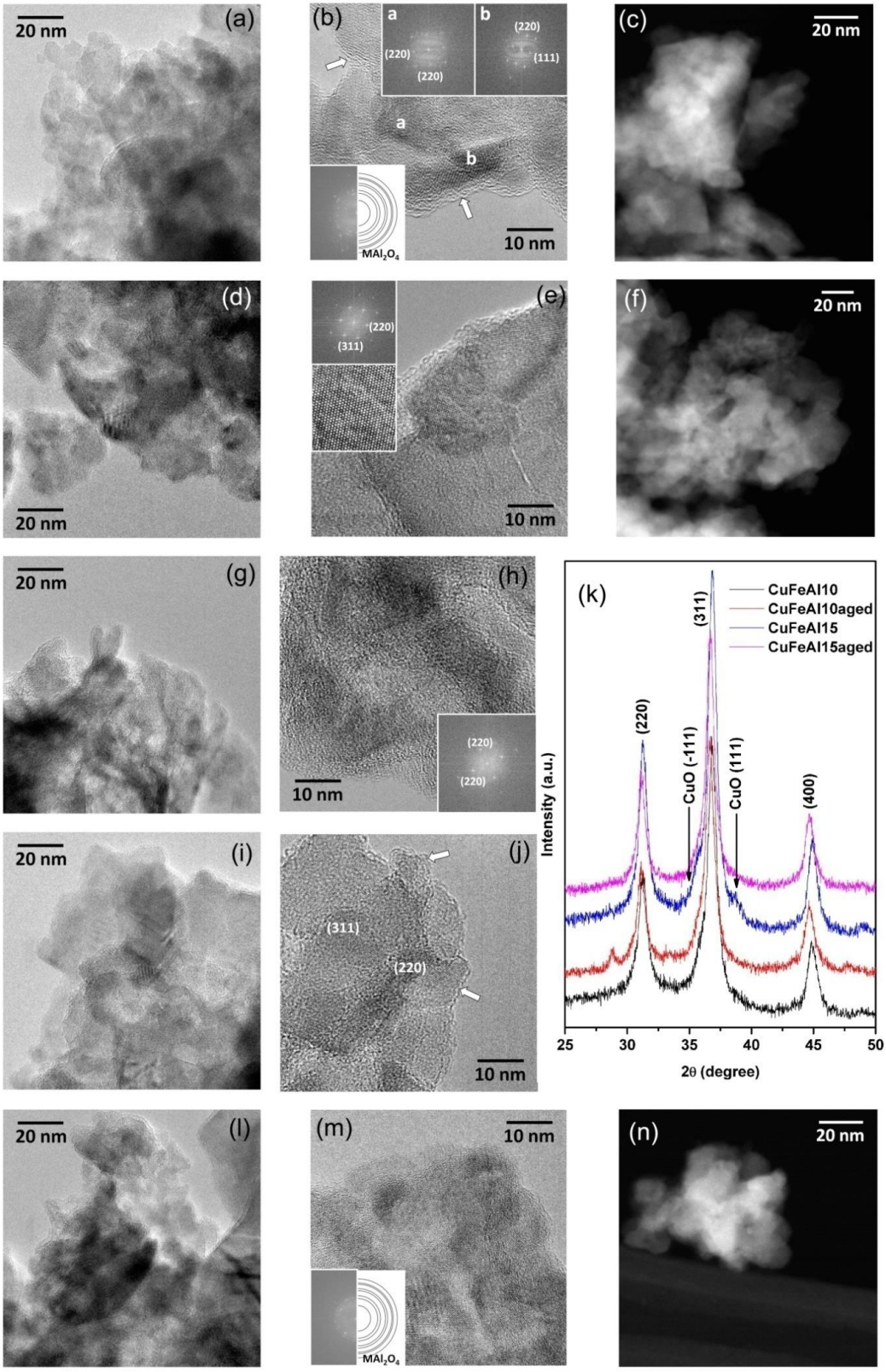
(a)
20 nm
(b)
a
b
(220)
(220)
(220)
(111)
a
b
10 nm
MAl2O4
(c)
20 nm
(d)
20 nm
(e)
(220)
(311)
10 nm
(f)
20 nm
(g)
20 nm
(h)
10 nm
(220)
(220)
(k)
CuFeAl10
CuFeAl10aged
CuFeAl15
CuFeAl15aged
(311)
(220)
CuO (-111)
CuO (111)
(400)
Intensity (a.u.)
25
30
35
40
45
50
2θ (degree)
(i)
20 nm
(j)
(311)
(220)
10 nm
(l)
20 nm
(m)
10 nm
MAl2O4
(n)
20 nm

Fig. 6

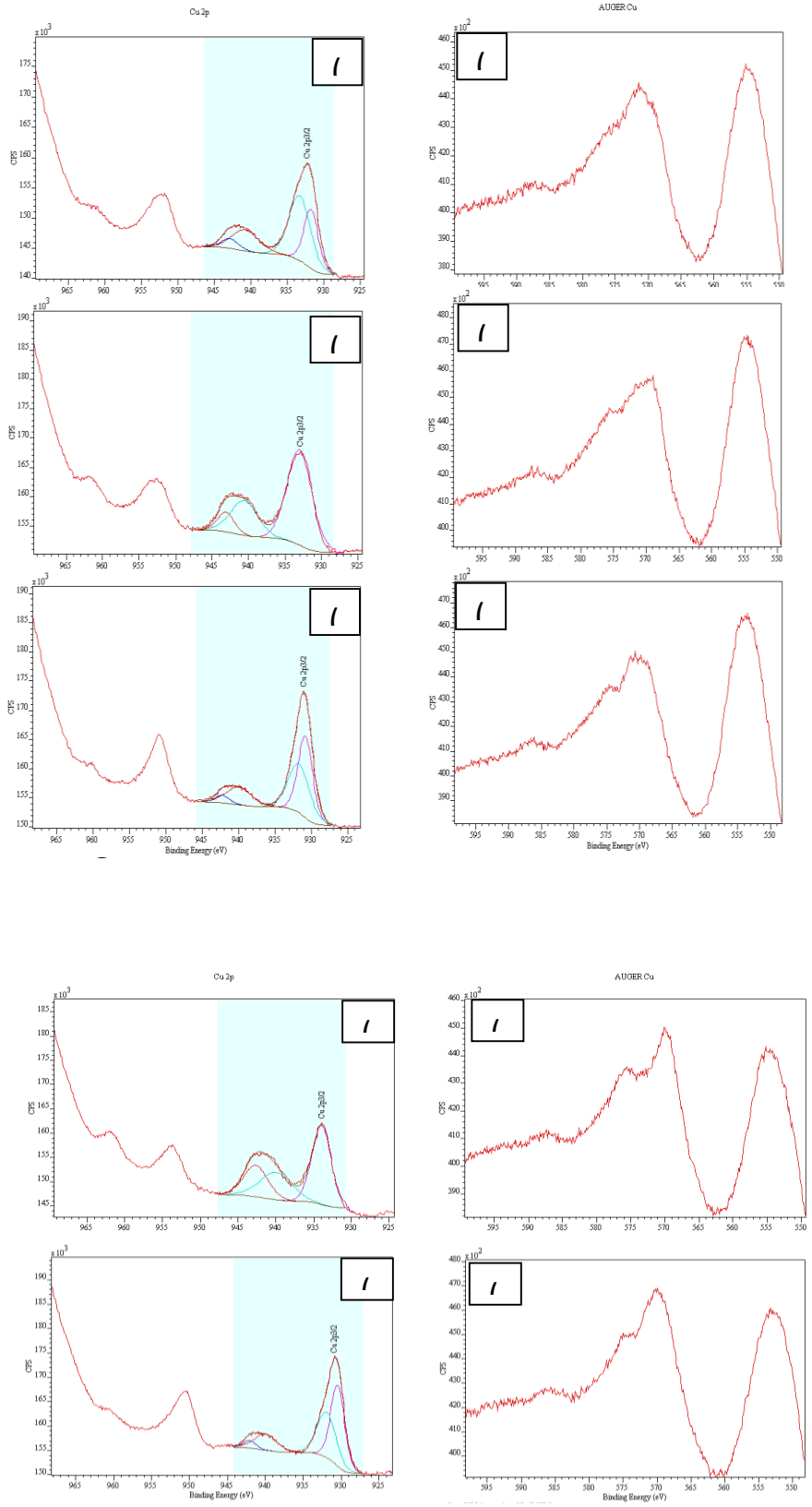

Fig. 8